ELSEVIER

Materials Science and Engineering A325 (2002) 497–502

MATERIALS SCIENCE & ENGINEERING A

www.elsevier.com/locate/msea

Ultra-precision machining induced surface structural changes of Zn–Al alloy

S. To [a], W.B. Lee [a], Y.H. Zhu [a,b,*]

[a] *Department of Manufacturing Engineering, The Hong Kong Polytechnic University, Hong Kong, PR China*
[b] *Instituto de Investigaciones en Materiales, Univ. Nacional Autonoma de Mexico, Apartado Postal 70-360, Mexico, DF 04510, Mexico*

Received 27 November 2000; received in revised form 13 July 2001

Abstract

Ultra-precision machining was carried out on a furnace cooled (FC) eutectoid Zn–Al alloy specimen using a new technology of single point diamond turning (SPDT). Microstructural changes and phase decomposition at the surface of the ultra-precision machined alloy specimen were investigated. It was found that the ultra-precision machining induced external stress resulted in decomposition of the ε phase and crystal orientation changes of the Zn-rich phases: η and ε, at the surface of the machined FC Zn–Al alloy specimen, which were in agreement with the tensile stress induced phase transformations and crystal orientation changes in the FC Zn–Al alloy specimen.

Keywords: Ultra-precision machining; Phase decomposition; Tensile deformation; Zn–Al alloys

1. Introduction

Ultra-precision machining has become an essential process in modern manufacturing industry. A new technology, named of single point diamond turning (SPDT), is applied in the ultra-precision machining to obtain a super mirror surface directly on non-ferrous metallic materials.

The properties of the free surface and the sub-surface of a machined metallic workpiece were known to be dependent on machining procedures and physical states of the workpiece. It was reported that surface microtexture of the workpiece had changed after face milling and flat grinding [1,2] The cutting behavior and mechanism of chip formation are known to be dependent on the crystallographic factors, such as crystal orientation, slip system and mobile dislocation density of the workpiece. The effect of the crystal orientation on the cutting mechanism of single crystal has received considerable research interest [3,4].

However, limited research has been done on the effect of ultra-precision machining on the material properties, and the understanding of microstructure and physical metallurgy of actual degenerated surface layer of the diamond machined workpieces, such as stress induced microstructural change and phase transformation, is even more limited [5–8]. Further research is clearly needed to provide this understanding.

The present paper will deal with the effect of the ultra-precision machining on the microstructural change and phase decomposition of the surface of a Zn–Al alloy, based on the systematic investigations of the alloy [9–11].

2. Experimental procedures

A cast ingot of an eutectoid alloy 76wt.%Zn–22wt.%Al–2wt.%Cu was prepared from high-purity materials (99.99% Zn, 99.99% Al and 99.99% Cu) and melted in a graphite crucible, in an induction furnace. The melt was degassed with zinc chloride ($ZnCl_2$) and cast at 700 °C into a preheated mild steel mould. The cast ingot was solution treated at 350 °C for 4 days and then furnace cooled at room temperature.

* Corresponding author. Tel.: +52-5-622-4641; fax: +52-5-616-1371.
E-mail address: yaohuazhu@hotmail.com (Y.H. Zhu).

0921-5093/02/$ - see front matter
PII: S0921-5093(01)01753-1

The furnace cooled (FC) Zn–Al alloy ingot was machined into cylindrical specimens of 10 mm in diameter with 8 mm height. The ultra-precision cutting were performed on a two-axis CNC ultra-precision diamond turning machine made by Taylor Hobson Pneumo Co. (Nanoform 300). The machine utilized precision dovetail slides and high speed air bearing spindle with an integral AC drive Motor. The slides were mounted on a natural granite base in a 'T' configuration, where the X-axis slide was the cross arm of the T and supported a dual tool holder assembly. The Z-axis slide was the stem of the T. The total slide travel was 150 mm on the X-axis and 100 mm on the Z-axis. Spindle rotation speed was infinitely variable from 100 to 3000 rpm with alliteration and deceleration times of less than 5 s.

Table 1
Cutting conditions for ultra-precision machining

Cutting speed	3000 rpm
Feed rate	20 mm/min
Depth of cut	1 μm
Tool rake angle	0°
Tool nose radius	0.534 mm
Front clearance angle	5°

The cutting conditions used in the ultra-precision machining are listed in Table 1.

An interferometric microscope (WYKO TOPO 3D) was used to measure the microsurface roughness. The first order statistical parameters, such as the average height (RA), root mean square height (RMS), and the higher order statistical parameters, such as slop, curvature, power spectrum and autocovariance function was obtained.

Standard metallographic examination was carried out on both bulk part of the specimen and surface of the ultra-precision machined specimen in a back scattered electron micorscope (BSEM) to attain atomic number contrast. Electron back-scattered diffraction (EBSD) was applied for examination of microstructure and microtexture of the ultra-precision machined specimens. EBSD was carried out in a stereo scan SEM operating at an accelerating voltage of 20 keV with specimen tilted at 70°, using a commercially available software (supplied by the Company HKL Technology APS).

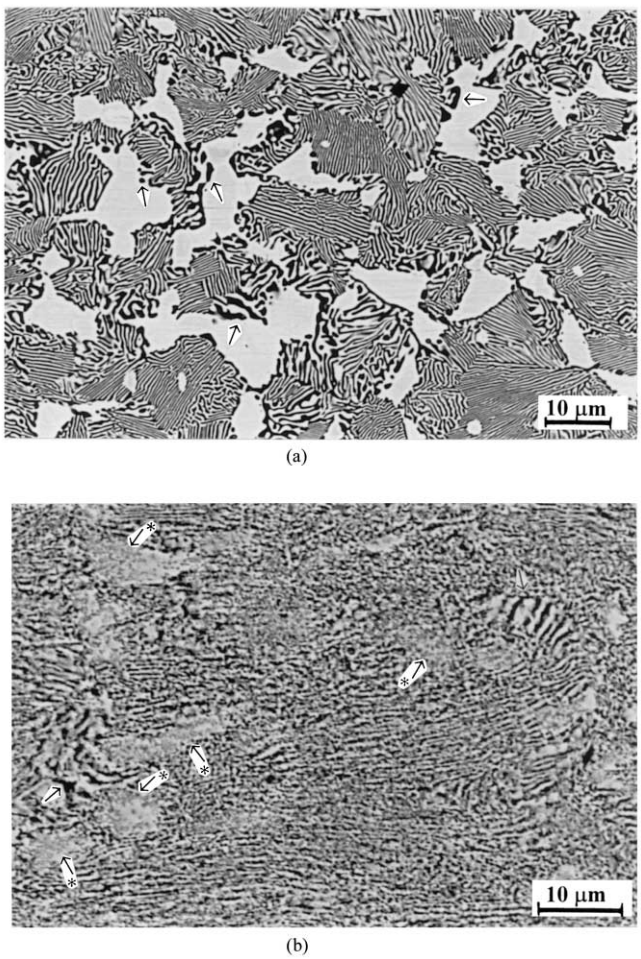

Fig. 1. BSEM images of the bulk part (a) and the surface (b) of the ultra-precision machined Zn–Al alloy specimen. →precipitate of α phase in η phase, * →precipitate of T' phase in ε phase.

3. Results

The micorstructures of both the bulk part and the surface of the ultra-precision machined FC Zn–Al alloy are shown in Fig. 1a and b. Typical microstructure of the FC Zn–Al alloy consisted of a corsened lammellar structure (thickness of lamellae, about 0.4 μm) and a fine lamellar structure (thickness of lamellae, about 0.14 μm), and light contrasted particles of two Zn-rich phases: η and ε, as shown in BSEM image, Fig. 1a. Also, dark contrasted precipitates were observed in the decomposoed Zn-rich η phase in the FC alloy, as indicated by arrows '→'.

In comparison, the BSEM image of the surface of the machined alloy both the corsened and fine lamellar structures were aligned along with the cutting track, as shown in Fig. 1b. In addition to the dark contrasted precipitates in the Zn-rich phases particles, gray precipitates were observed at the light contrasted ε phase particles, as arrows '* →' pointed in Fig. 1b.

From previous investigations, [9–11] it was recognized that the dark contrasted precipitates were Al-rich phase, which was from the decomposition of the Zn-rich η phase. The gray precipitates were T' phase, as one of the products of the decomposition of the ε phase via a four-phase transformation: $\alpha + \varepsilon \rightarrow T' + \eta$.

The Zn-rich η and ε phases were identified using EBSD mapping, as shown in Fig. 2a and b. Both pre-determined lattice parameters of the η and ε phases

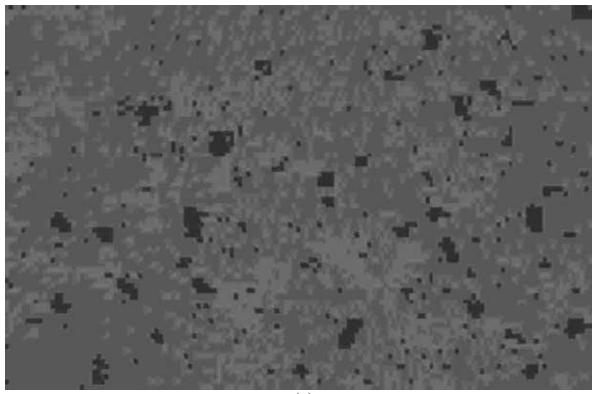
(a)

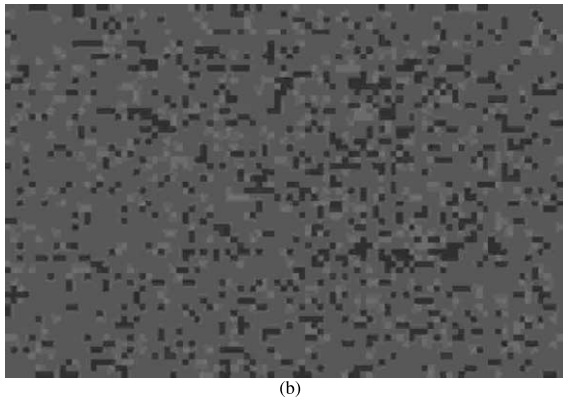
(b)

Fig. 2. EBSD mapping of η and ε phases of the bulk part (a) and the surface (b) of the ultra-precision machined Zn–Al alloy specimen.

were applied as preset database for EBSD [12]. The Zn-rich η and ε phases of similar hcp crystal structures were distinguished from each other. The gray area is the undetected lamellar structures. The light-imaged area and the dark-imaged area are two Zn-rich phases: η and ε, respectively. During the ultra-precision machining, i.e. the single point diamond turning (SPDT), the cutting is performed within each individual crystals. Fine dispersive images of both the η and ε phase particles were observed in the EBSD mapping of the surface of the machined alloy specimen, as shown in Fig. 2b.

In performing an EBSD investigation, it is easier to correlate grains/orientations on an inverse pole figure than a pole figure because in the former there is only one project point per grain, whereas in a pole figure there are at least three. Thus the inverse pole figure is always applied for indicating the preferred orientation of the phases involved. Shown in Fig. 3a and b are the inverse pole figures of η phase of the bulk part and the surface of the ultra-precision machined FC Zn–Al alloy specimen, respectively. It was clear that majority of the project points of the η phase were located at about (0001) planes in the bulk part of the FC alloy specimen, as shown in Fig. 3a. While the the project points of the η phase were despersed away from the (0001) planes at the surface of the ultra-pecision machined alloy specimen, as shown in Fig. 3b.

The inverse pole figures of the ε phase of the bulk part and the surface of the ultra-precision machined FC Zn–Al alloy specimen are shown in Fig. 4a and b, respectively. The project points of the ε phase of the bulk part of the FC alloy specimen were mainly located at about (0001) and $(10\bar{1}0)$ planes, as shown in Fig. 4a. After ultra-precision machining, the project points of the ε phase disappeared from about $(10\bar{1}0)$ planes and remained dispersively at about (0001) planes and the amount of the project points decreased considerably, as show in Fig. 4b.

4. Discussion

4.1. Stress induced phase transformation

The decomposition of the η phase and the four-phase transformation: $\alpha + \varepsilon \rightarrow T' + \eta$, have been detected repeatedly in the eutectoid Zn–Al alloy specimen during various thermomechanical treatments [9–11]. The typi-

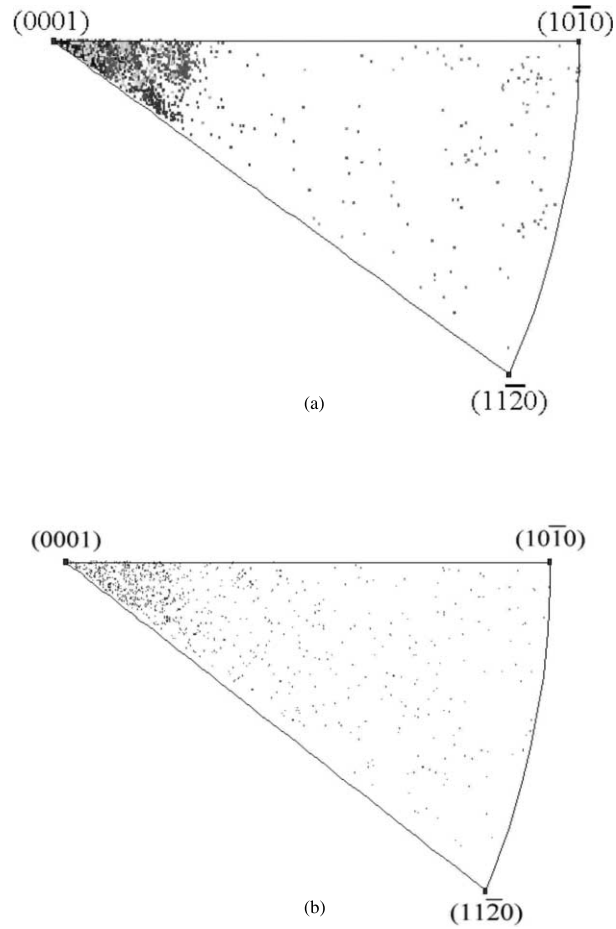

Fig. 3. Inverse pole figure of η phase of the bulk part (a) and the surface (b) of the ultra-precision machined FC Zn–Al alloy specimen.

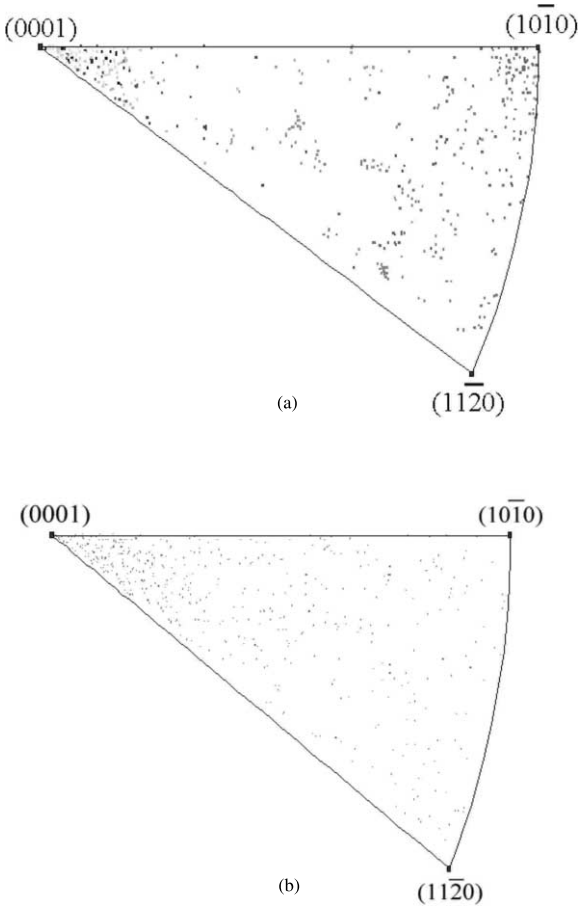

Fig. 4. Inverse pole figure of ε phase of the bulk part (a) and the surface (b) of the ultra-precision machined FC Zn–Al alloy specimen.

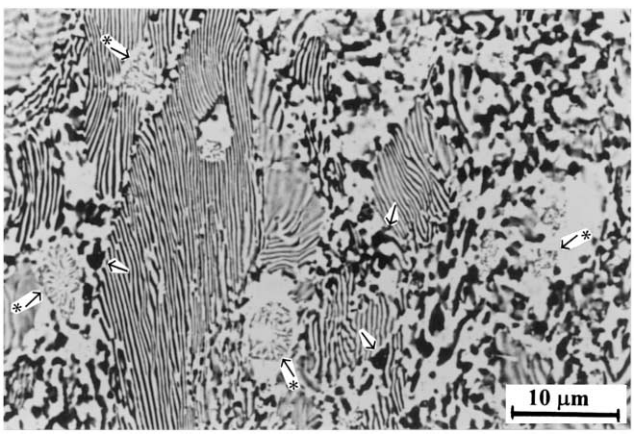

Fig. 5. BSEM image of rupture part of the tensile tested FC ZA22 alloy specimen. →precipitate of α phase in η phase, * →precipitate of T' phase in ε phase.

cal morphologies of the above mentioned phase transformations were also reported in the previous investigations.

For comparison, the BSEM image of a rupture part of the tensile tested FC eutectoid Zn–Al alloy specimen is shown in Fig. 5 [13]. During tensile deformation, the coarse lamellar structure in the FC Zn–Al alloy specimen segmented into particulate structure. The segmentation of the coarse lamellar structure became obvious in the rupture part of the tensile tested specimen. While the fine lamellar structure withstood the external strain and remained unchanged. Both the precipitates of the α and the T' phase inside the η and ε phases are indicated by arrows of '→' and '*→' in Fig. 5, respectively. Under tensile deformation, the gray precipitates of the T' phase was clearly observed in the rupture part of the tensile tested FC Zn–Al alloy specimen, i.e. the concentrated tensile stress induced the decomposition of the ε phase in the FC Zn–Al alloy.

From the BSEM images of the ultra-precision machined FC Zn–Al alloy, Fig. 1, it was obvious that the gray T' phase precipitates inside the ε phase formed at the surface of the specimen during ultra-precision machining. That implied that the above mentioned decomposition of the ε phase, i.e. four-phase transformation: $\alpha + \varepsilon \rightarrow T' + \eta$, was induced by an external stress during ultra-precision machining. In other words, ultra-precision machining induced an external stress that accelerated the decomposition of the ε phase at the surface of the machined specimen. In the absence of deformation the transformation is very slow, e.g. at 150 °C a similar alloy was heat-treated for 30 h to half complete the reaction [11].

4.2. Stress induced microstructural changes

During ultra-precision machining, the depth of cutting is often smaller than the grain size of the polycrystalline materials, thus both the corsened and fine lamellar structures were aligned with the cutting track and partly destroyed to dispersive particles and segments. In consequence, an external stress was induced at the surface of the machined alloy.

In previous studies, [13] it was reported that external stresses resulted in change of preferred orientation of phases in the Zn–Al alloys.

After solution treatment and furnace cooling, internal strain became very small, and the project points in the inverse pole figure of the η phase were concentrated at about (0001) planes, as shown in Fig. 3a. For comparison, the inverse pole figures of the rupture part and the neck zone of the tensile tested FC eutectoid Zn–Al alloy speciemn is shown in Fig. 6 and Fig. 7. The project points of the η phase became more dispersive away from (0001) planes when the distance from the rupture frontier was decreased, as shown in Fig. 6a and b. Obviously, the crystal orientation changes of the η phase were caused by increasing of tensile stress.

In the ultra-precision machine FC Zn–Al alloy specimen, a similar stress induced crystal orientation change was observed. As can be seen in Fig. 3b, the project points in the inverse pole figure of the η phase at the

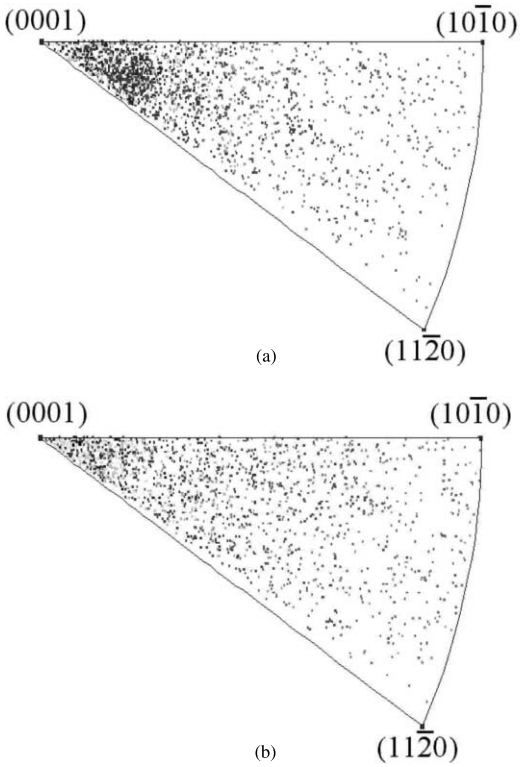

Fig. 6. Inverse pole figure of η phase of neck (a) and rupture (b) parts of the tensile tested FC Zn–Al alloy specimen.

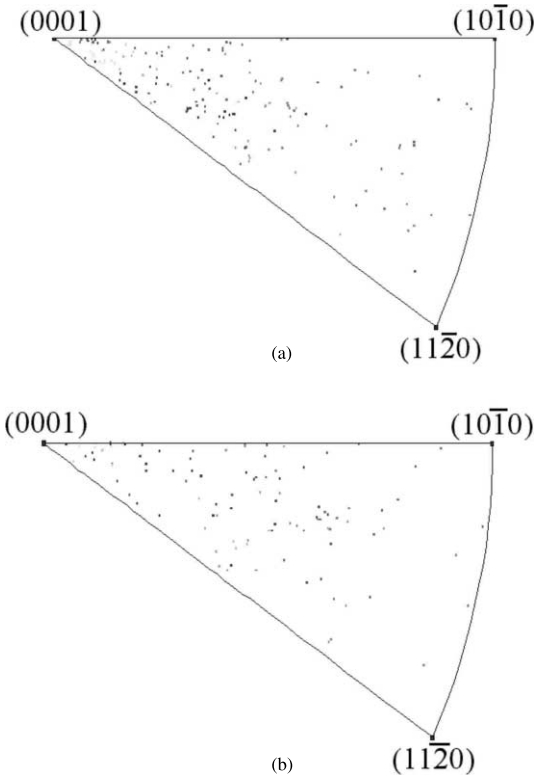

Fig. 7. Inverse pole figure of ε phase of neck (a) and rupture (b) parts of the tensile tested FC Zn–Al alloy specimen.

surface of the machined alloy specimen had been dispersive away from the (0001) planes.

The crystal orientation changes of the ε phase induced by the ultra-precision machining, were clearly shown in Fig. 4a and b. Most project points in the inverse pole figure of the ε phase in the FC Zn–Al alloy specimen were located at about (0001) and (10$\bar{1}$0) planes, shown in Fig. 4a, while the project points in the inverse pole figure of the ε phase disappeared at about (10$\bar{1}$0) at the surface of the machined FC Zn–Al alloy specimen, shown in Fig. 4b.

The ultra-precision machining induced crystal orientation changes of the ε phase were also observed in the tensile tested FC Zn–Al alloy specimen. For comparison, the inverse pole figure of the ε phase in the rupture part and the neck zone of the tensile tested FC Zn–Al alloy specimen is shown in Fig. 6b [13]. It is found that the project points in the inverse pole figure of the ε phase disappeared from (10$\bar{1}$0) planes in the rupture part and the neck zone of the specimen because of the high stress. Meanwhile the amount of the project points decreased considerably. It was because with increasing of the external stress, the decomposition of the ε phase developed. This implied that the ultra-precision machining induced crystal orientation changes of the ε phase at the surface of the FC Zn–Al alloy spcecimen were, in fact, a kind of the external stresse induced crystal orientation changes.

5. Conclusions

Ultra-precision machining induced external stress accelerated the decomposition of the ε phase at the surface of the machined FC Zn–Al alloy. Meanwhile, both the corsened and fine lamellar structures were aligned with the cutting track and partly destroyed to dispersive articles and segments at the surface of the machined alloy specimen.

Ultra-precision machining induced external stress resulted in crystal orientation change of the Zn-rich phases: η and ε, which was in agreement with the tensile stress induced crystal orientation changes in the FC Zn–Al alloy specimen.

Acknowledgements

The authors would like to express their greatfulness to T.K. Cheung for his help in the experimental work.

References

[1] H. Krause, E. Vcalan, In: C.M. Brakman, P. Jongenburger, E.J. Mittmeijer (Eds.), Proceedings of the Seventh International Conference on Texture of Materials, 1984, pp. 625.

[2] G. Maurer, H. Neff, B. Scholtes, E. Macherauch, Textures and Microstructures, 8 & 9, pp. 639, 1988, Xian, China, 16–20 September, 1996, pp. 293–298.
[3] K. Ueda, K. Iwata, Ann. CIRP 29 (1980) 41.
[4] Z.J. Yuan, W.B. Lee, Y.X. Yao, M. Zhou, Ann. CIRP 43 (1994) 39.
[5] J.H. Zhang, Theory and Technique of Precision Cutting, Pergamon Press, New York, 1991.
[6] Z.J. Yuen, M. Zhou, S. Dong, J. Mat. Process. Technol. 62 (1996) 327.
[7] S. To, W.B. Lee, C.Y. Chan, Textures Microstruct. 31 (1999) 249.
[8] W.B. Lee, S. To, C.Y. Chan, Lattice rotation in machining aluminium single crystal, Proceedings of Eleventh International Conference on Texture of Materials, Xian, China, 16–20 September, 1996, pp. 293–298.
[9] Y.H. Zhu, J. Mater. Sci. in press.
[10] Y.H. Zhu, Metals Maters 4 (1998) 878–882.
[11] Y.H. Zhu, W.B. Lee, Mater. Sci. Eng. A 293 (2000) 95–101.
[12] Y.H. Zhu, W.B. Lee, C.F. Yeung, T.M. Tue, Mater. Charact. 46 (2001) 19–23.
[13] Y.H. Zhu, W.B. Lee, to be published.